

# The Deuterium Abundance in the $z = 0.7$ absorber towards QSO PG1718+4807

N. H. M. Crighton, J. K. Webb, R. F. Carswell and K. M. Lanzetta

## ABSTRACT

We report a further analysis of the ratio of deuterium to hydrogen (D/H) using HST spectra of the  $z = 0.701$  Lyman limit system towards the QSO PG1718+481. Initial analyses of this absorber found it gave a high D/H value,  $1.8 - 3.1 \times 10^{-4}$  (Webb et al. 1998), inconsistent with several higher redshift measurements. It is thus important to critically examine this measurement. By analysing the velocity widths of the D I, H I and metal lines present in this system, Kirkman et al. (2001) report that the additional absorption in the blue wing of the Ly $\alpha$  line can not be D I, with a confidence level of 98%. Here we present a more detailed analysis, taking into account possible wavelength shifts between the three sets of HST spectra used in the analysis. We find that the constraints on this system are not as strong as those claimed by Kirkman et al. (2001). The discrepancy between the parameters of the blue wing absorption and the parameters expected for D I is marginally worse than  $1\sigma$ .

Tytler et al. (1999) commented on the first analysis of Webb et al. (1997, 1998), reporting the presence of a contaminating lower redshift Lyman limit system, with  $\log[N(\text{H I})] = 16.7$  at  $z = 0.602$ , which biases the  $N(\text{H I})$  estimate for the main system. Here we show that this absorber actually has  $\log[N(\text{H I})] < 14.6$  and does not impact on the estimate of  $N(\text{H I})$  in the system of interest at  $z = 0.701$ .

The purpose of the present paper is to highlight important aspects of the analysis which were not explored in previous studies, and hence help refine the methods used in future analyses of D/H in quasar spectra.

## Key words:

## 1 INTRODUCTION

Virtually all the deuterium (D) and the vast majority of H and  $^4\text{He}$  we observe today were produced during big bang nucleosynthesis (BBN). BBN also produced small amounts of  $^3\text{He}$  and  $^7\text{Li}$ . In standard BBN theory, the primordial abundances of all these light elements depends solely on the cosmological baryon density,  $\Omega_b$ . This allows  $\Omega_b h^2$  to be measured directly by finding the primordial ratio of any two of these light elements<sup>1</sup>. The ratio D/H is very sensitive to  $\Omega_b h^2$ , and of all the BBN light elements, D/H potentially gives the best constraints on  $\Omega_b$ .

QSO absorption systems provide a unique way to measure the primordial abundance of deuterium (Adams 1976). Theoretically there are processes other than BBN that create D, but it has been shown (Epstein, Lattimer & Schramm 1974) that the D production due to these processes is likely to be negligible compared to D production during BBN (but see also Jedamzik 2002). Stellar nuclear reactions cause a net destruction

of D, so measurements of the D abundance in sites that have undergone star formation, such as our Galaxy, provide a lower limit to the primordial D/H value. However, many QSO absorption clouds are thought to have undergone very little star formation, and we expect D/H in these clouds to be close to the primordial value. Unfortunately, very few absorption systems have the high column density ( $\geq 10^{17}$  absorbers per  $\text{cm}^2$ ), simple velocity structure and narrow linewidth that are required for the D I line to be separated from the nearby H I absorption (Webb, Carswell, Irwin & Penston 1991).

Most existing D/H measurements have been made in absorption systems with a redshift large enough that the Lyman limit falls in the visible ( $z > 2.2$ ). For lower redshift systems the Lyman limit falls in the UV and must be observed from space. However, it is desirable to look for low redshift systems as there is a much larger sample of bright QSOs at lower redshifts. In addition, the number density of Ly $\alpha$  forest absorbers is much lower at low redshifts compared to high redshifts. This means it is easier to accurately measure the continuum level around the relevant absorption

<sup>1</sup>  $h \equiv \frac{1}{100 \text{ km s}^{-1} \text{Mpc}^{-1}} \times (\text{Hubble constant})$

lines, and the chance of a randomly placed H<sub>I</sub> line contaminating the D<sub>I</sub> absorption is smaller.

The absorption system at  $z = 0.701$  towards PG1718+4807 was first identified as an excellent candidate for a D/H measurement from an International Ultraviolet Explorer (IUE) spectrum covering its Lyman limit (LL). Its LL is ‘grey’, meaning the flux does not drop to zero bluewards of the LL. The drop in flux at the grey LL strongly constrains the column density of the absorber. The column density was high enough for the D<sub>I</sub> Ly $\alpha$  line to be detected, and the sharp break at the LL suggested the velocity structure of the absorption complex was very simple. Webb, Carswell, Lanzetta, Ferlet, Lemoine, Vidal-Madjar & Bowen (1997) published the first analysis of D/H in the  $z = 0.701$  system, using a GHRS spectrum covering the Ly $\alpha$  and Si III lines and the IUE spectrum covering the LL. Webb et al. (1997, 1998) fitted the H<sub>I</sub> absorption with a single cloud, assuming the redshift of the Si III line was the same as the redshift of the H<sub>I</sub> absorption. They found D/H of  $1.8 - 3.1 \times 10^{-4}$ , about ten times higher than D/H measured in other, higher redshift absorption systems ( $\sim 2 - 4 \times 10^{-5}$ , see O’Meara, Tytler, Kirkman, Suzuki, Prochaska, Lubin & Wolfe 2001; Pettini & Bowen 2001; Levshakov, Dessauges-Zavadsky, D’Odorico & Molaro 2002; Kirkman, Tytler, Suzuki, O’Meara & Lubin 2003).

Tytler, Burles, Lu, Fan, Wolfe & Savage (1999) subsequently published a further analysis of D/H in the same absorber, adding Keck/HIRES spectra of Mg II lines associated with the  $z = 0.701$  absorber. Using the Mg II lines they considered several models with different constraints on the H<sub>I</sub> component’s redshift. They found a larger range of D/H:  $8 - 57 \times 10^{-5}$ .

Kirkman, Tytler, O’Meara, Burles, Lubin, Suzuki, Carswell (2001) (hereafter KTOB) published new HST STIS (Space Telescope Imaging Spectrograph) spectra covering the LL, Ly $\alpha$  and Si III lines of the absorber. The spectrum of the LL has a resolution of  $10 \text{ kms}^{-1}$ , and all the Lyman series lines from Lyman- $\epsilon$  to Lyman-16 were resolved (see Fig. 1). This spectrum confirmed the presence of a single *strong* H<sub>I</sub> component and allowed its redshift to be measured precisely. However, Kirkman et al. (2001) found additional *weak* absorption to the red of the main H<sub>I</sub> component. This absorption was too weak to be seen in the higher order Lyman series, but was seen in the new STIS spectrum of the Ly $\alpha$  line. They also claimed that the  $b$  parameter ( $b = \sqrt{2}\sigma$ , where  $\sigma$  is the velocity dispersion) of the putative D<sub>I</sub> was larger than that expected for a gas with a temperature and turbulence calculated from the H<sub>I</sub> and metal lines’  $b$  parameters. Based on these two points they claimed that the absorption fitted as D<sub>I</sub> in Webb et al. (1997) and Tytler et al. (1999) is contaminated by weak H<sub>I</sub> absorption. Due to this contamination they concluded the system does not provide evidence for a high D/H value.

We present a further analysis of D/H in the  $z = 0.701$  absorption system, in which we look at the effect of systematic errors, not addressed in previous analyses, that affect the  $z = 0.701$  absorption system parameters. In particular we analyse how the putative D<sub>I</sub> absorption’s parameters are affected by wavelength calibration errors in the HST spectra and present revised parameters for this particular absorption spectrum. These calibration effects will be

important for future analyses of D/H in QSO spectra. Finally, we assess the likelihood that this absorption system shows D<sub>I</sub> and give an estimate of D/H for this system.

## 2 DATA AND ANALYSIS

The QSO PG1718+4807 has been observed with the Faint Object Spectrograph (FOS), Goddard High Resolution Spectrograph (GHRS) and STIS on the HST, and the IUE (Lanzetta, Turnshek & Sandoval 1993)<sup>2</sup>. We are interested in finding the parameters of the H<sub>I</sub> and D<sub>I</sub> absorption. The resolutions of the FOS and IUE spectra are much lower (FWHM  $\sim 150$  and  $\sim 900 \text{ kms}^{-1}$  respectively) than those of the GHRS and STIS spectra. The FOS and IUE spectra do not provide any useful constraints on the parameters of D<sub>I</sub> or any H<sub>I</sub> sub-components which may be present in the  $z = 0.701$  absorption complex. The parameters of the main H<sub>I</sub> component are very well determined by the STIS spectra alone (see section 2.8). Therefore we use only the GHRS and STIS spectra in our analysis.

Tytler et al. (1999) detected Mg II with Keck/HIRES. We use their best fitting parameters for Mg II, with a modified error for the Mg II  $b$  parameter (see section 2.8).

### 2.1 GHRS data

The GHRS spectra were taken using the G140M grating with a  $0.2 \times 0.2$  aperture giving a line spread function (LSF) with a FWHM of  $14 \text{ kms}^{-1}$ . The observations consisted of 56 exposures, which were shifted and added using the IRAF routines written for this purpose by the Space Telescope Science Institute (STScI), *poffsets* and *specalign*. We used the pipeline reduced spectra, processed with CALHRS version 1.3.13. The wavelength range covered is  $2049 - 2098 \text{ \AA}$ . The S/N per pixel near the Ly $\alpha$  and Si III lines in the combined spectrum is  $\sim 10$ .

### 2.2 STIS data

The STIS observations were taken with the E230M echelle grating and the G140M longslit grating with the  $0.2 \times 0.2$  aperture. The FWHM of each of the LSFs of the STIS observations are 2 pixels for the E230M echelle grating ( $5 \text{ kms}^{-1}$  per pixel) and 1.5 pixels for the G140M grating ( $0.06 \text{ \AA}$  or  $\sim 11 \text{ kms}^{-1}$  per pixel). Four exposures were taken with the G140M grating, and five with the E230M grating. In each case we used the pipeline reduced spectra (CALSTIS version 2.8). For each set of observations the exposures were rebinned to a common wavelength scale and combined using a variance weighted average. The E230M spectra cover the wavelength region  $1842 - 2673 \text{ \AA}$ . The final S/N per pixel near the Ly $\alpha$  and Si III lines in the averaged E230M spectrum is  $\sim 5$ . The G140M spectra cover the Lyman- $\epsilon$  transition down to the Lyman limit, a wavelength range of  $1540 - 1594 \text{ \AA}$ . The S/N per pixel in the G140M averaged spectrum is  $\sim 9$ .

<sup>2</sup> The GHRS, STIS, FOS and IUE spectra are all available from the HST multimission data archive: <http://archive.stsci.edu>

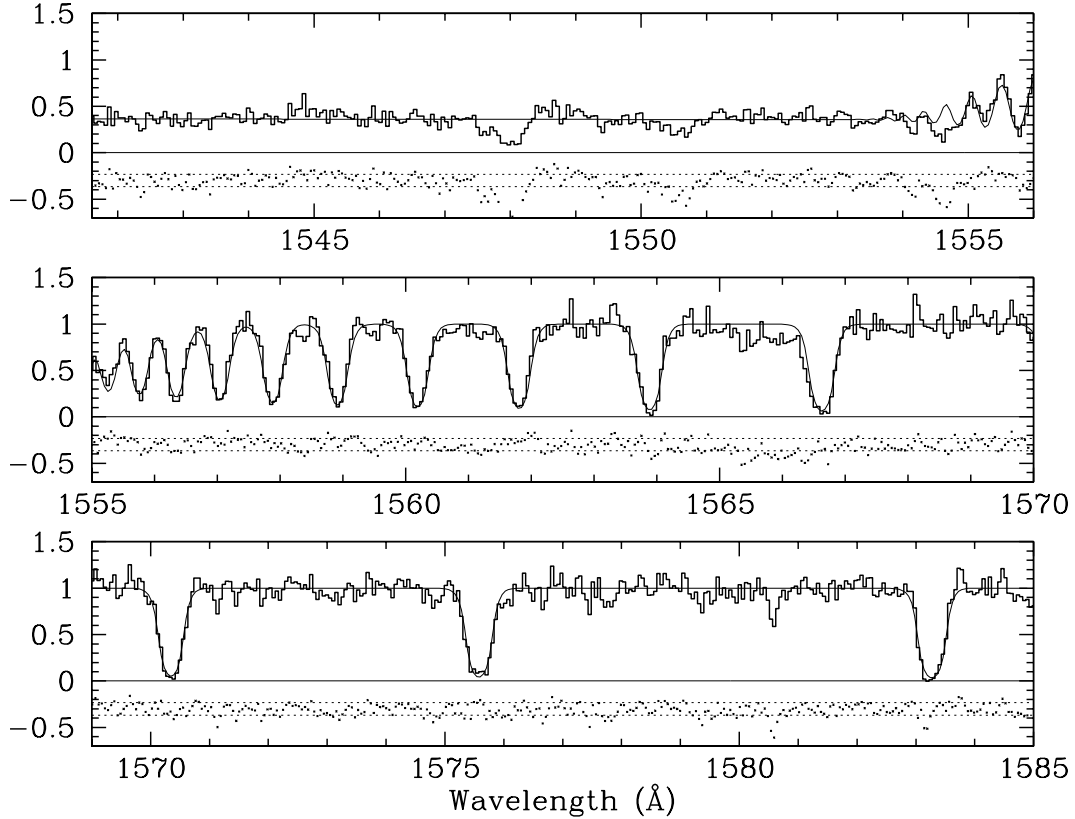


**Figure 1.** The STIS spectrum of the  $z = 0.701$  Lyman limit, a weighted sum of four STIS exposures with the G140M grating. There appears to be Galactic CIV absorption and emission at  $\sim 1548$  and  $\sim 1550.5$  Å. We are unsure what is causing the absorption at  $\sim 1554.5$ ,  $1565 - 1566.5$  and  $\sim 1580.5$  Å. Neither these regions, nor the regions affected by Galactic CIV absorption were included in the fit. The normalised residuals (which we define  $\equiv \frac{1}{15}(\text{data point} - \text{fitted value})/\text{error}$ ) and the  $1\sigma$  error levels for the residuals are shown centred on  $y = -0.3$ . The thin curve shows the best fitting solution when the Ly $\alpha$  lines and the LL are fit simultaneously. This fit provides the H $\text{I}$  parameters in Table 1.

### 2.3 Line spread functions

The LSF of the GHRS observations can be approximated by a Gaussian, but the STIS LSFs are significantly different from a Gaussian. We used the instrumental profiles for the E230M and G140M gratings given in the STIS instrument handbook<sup>3</sup>. The actual STIS LSFs may be slightly asymmetric. The nature of this asymmetry depends on the orientation of the slit on the sky (Sahu in KTOB). We averaged the asymmetric sides of the LSF to give a symmetric LSF for both the G140M and E230M gratings. We note that even if some small asymmetry is present, it will not have a significant effect on the fitted absorption line parameters. Once the LSF per pixel for the original spectrum was determined it was rebinned to the same wavelength scale as our final averaged spectrum. For the E230M grating, the pixels are a constant size in velocity rather than wavelength. We calculated an E230M LSF at the central wavelength of each line fitted in the E230M spectrum.

### 2.4 Continuum placement

The placement of the continuum in the STIS G140M spectrum has a potentially significant effect on the fitted  $b$  pa-

rameter and column density of the main H $\text{I}$  component. To test the magnitude of this effect, we fitted the continuum of this region using several methods. Firstly we fitted a constant flux to regions apparently free of absorption. Secondly we fitted a power law  $f_\lambda \propto \lambda^{-\alpha}$ . Finally, the IUE spectrum covers a larger wavelength range redwards of the Lyman limit than the STIS G140M spectrum, so it may give a better estimate of the continuum than just fitting the STIS Lyman limit. We fitted the IUE Lyman limit with a 3rd order Chebyshev polynomial and scaled this continuum to the level of the STIS Lyman limit, based on regions apparently free from absorption. Each of these methods gave very similar column densities and  $b$  parameters for the main H $\text{I}$  component. The small error due to continuum fitting was added in quadrature to the statistical error. This combined error is the first error given in Table 1.

<sup>3</sup> [http://www.stsci.edu/hst/stis/performance/spectral\\_resolution/](http://www.stsci.edu/hst/stis/performance/spectral_resolution/)

The error in continuum placement around the Ly $\alpha$  line, Si III line and  $\frac{1}{4}$  doublet (Fig. 2, 3 and 4) was determined by fitting both straight lines and 3rd order Chebyshev polynomials to regions apparently free from absorption close to each line. The differences between these two methods of continuum fitting have a negligible effect on the absorption line parameters.

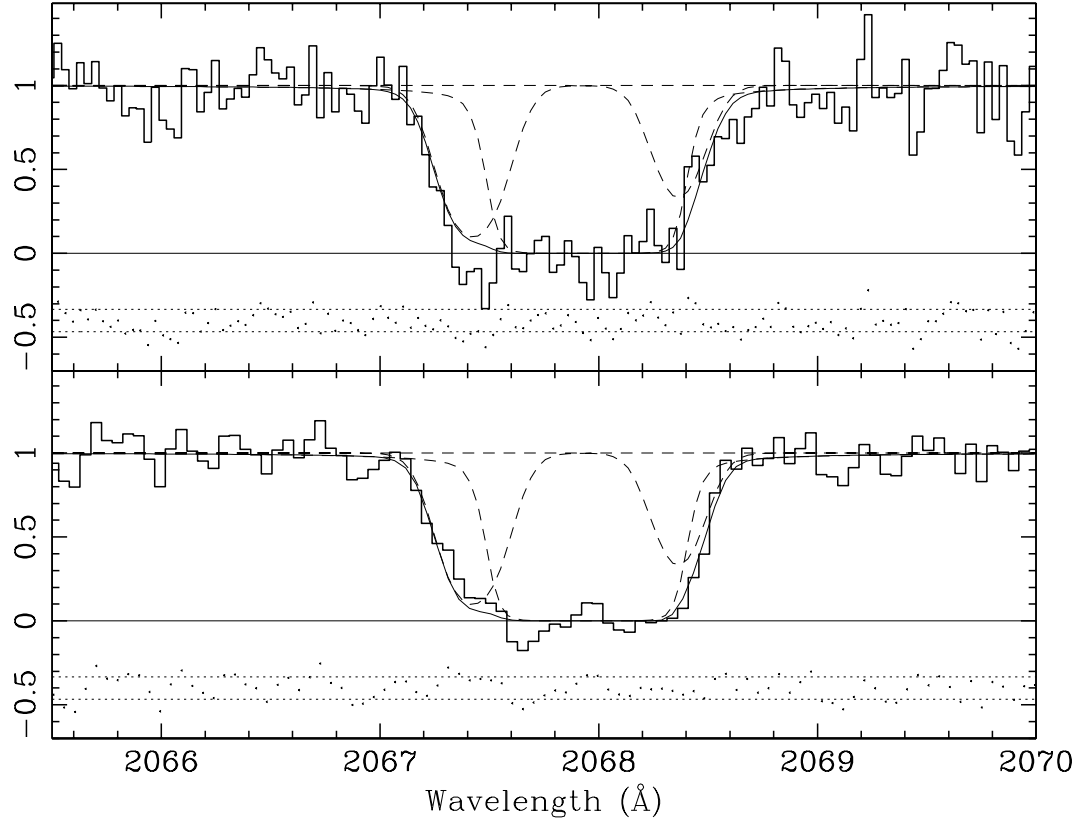


**Figure 2.** The GHRS (above) and STIS (below) spectra covering the  $z = 0.701$  Ly $\alpha$  line. The normalised residuals and their  $1\sigma$  error levels are shown centred on  $y = -0.4$ . The thin curve shows the best fitting solution when the Ly $\alpha$  lines and the Lyman limit are fit simultaneously. This fit provides the parameters in Table 1. The contributions from the main H $I$  component, red and blue components are shown by dashed curves. Note that the ‘shape’ of the STIS E230M Ly $\alpha$  line appears to be different to that of the GHRS line. In particular, the shape of the red wing and the absorption at  $\sim 2067.4$  Å are different. We are not certain what causes these differences, but they may be explained by correlations in the noise.

## 2.5 Wavelength calibration and shifts between the HST spectra

Misalignment of the wavelength scale between the GHRS, STIS G140M and STIS E230M spectra can potentially affect all the fitted parameters for H $I$  and the putative D $I$ , and the redshift for Si $III$  and 4.

The GHRS wavelength scale appears to be offset from the STIS wavelength scale by  $\sim 0.07$  Å ( $\sim 1.4$  GHRS pixels). Despite helpful discussion with Claus Leitherer from STScI we were unable to discover the reason for the discrepancy. KTOB shifted the GHRS spectrum to coincide with the STIS spectrum, finding the amount by which to shift by cross correlation over the common wavelengths covered. They then checked this shift by comparing the positions of profile fits to sharp features in each spectrum. However, they do not estimate the error in their shift.

We calculate the shift by choosing the three sharpest absorption features at relatively high S/N present in each spectrum and calculating the cross correlation for each of them. The regions we used were: 2051.1 – 2053.7 Å (the Si $III$  line), 2056.5 – 2060.4 Å (a Ly $\beta$  line at  $z = 1.0065$ ) and 2069.6 – 2072.2 Å (a Ly $\alpha$  line at  $z = 0.70326$ ). The three shifts for these regions were 0.070 Å, 0.072 Å and 0.058 Å respectively. The three shifts are roughly consistent, suggesting that the wavelength offset is the same across the

spectrum. We take the average of these three shifts and move the GHRS spectrum by this amount to align it with the STIS spectrum, assuming that the STIS wavelength calibration is more accurate than the the GHRS calibration. To quantify the error in this shift, we fit the sharpest feature in each spectrum, the Si $III$  line, with VPFIT. The VPFIT errors in the position of each line were then added in quadrature to give an estimate of the total error in the shift. This error is  $\sim 0.007$  Å, or  $\sim 1$   $\text{km s}^{-1}$ . This error does not have a significant effect on the the parameters of the putative D $I$  or main H $I$  absorption.

For a  $0.2 \times 0.2$  aperture and the MAMA detector used for the STIS observations, the absolute wavelength calibration error can be as much as 0.5 – 1.0 pixels ( $2\sigma$ , Proffitt 2002). In our analysis we introduce a conservative error of 0.3 pixels in the G140M and E230M wavelength calibrations. Thus we consider three different cases: (1) The wavelength calibration of both the G140M and E230M spectra are both correct, (2) the E230M spectrum wavelength scale shifted 0.3 pixels bluewards and the G140M wavelength scale 0.3 pixels redwards, and (3) the E230M wavelength scale shifted 0.3 pixels redwards and the G140M scale 0.3 pixels bluewards. Introducing even these conservative relative shifts of 0.6 pixels between the STIS E230M and G140M spectra does have a significant effect on the absorption line parameters, particularly those of the putative D $I$ . This is because the

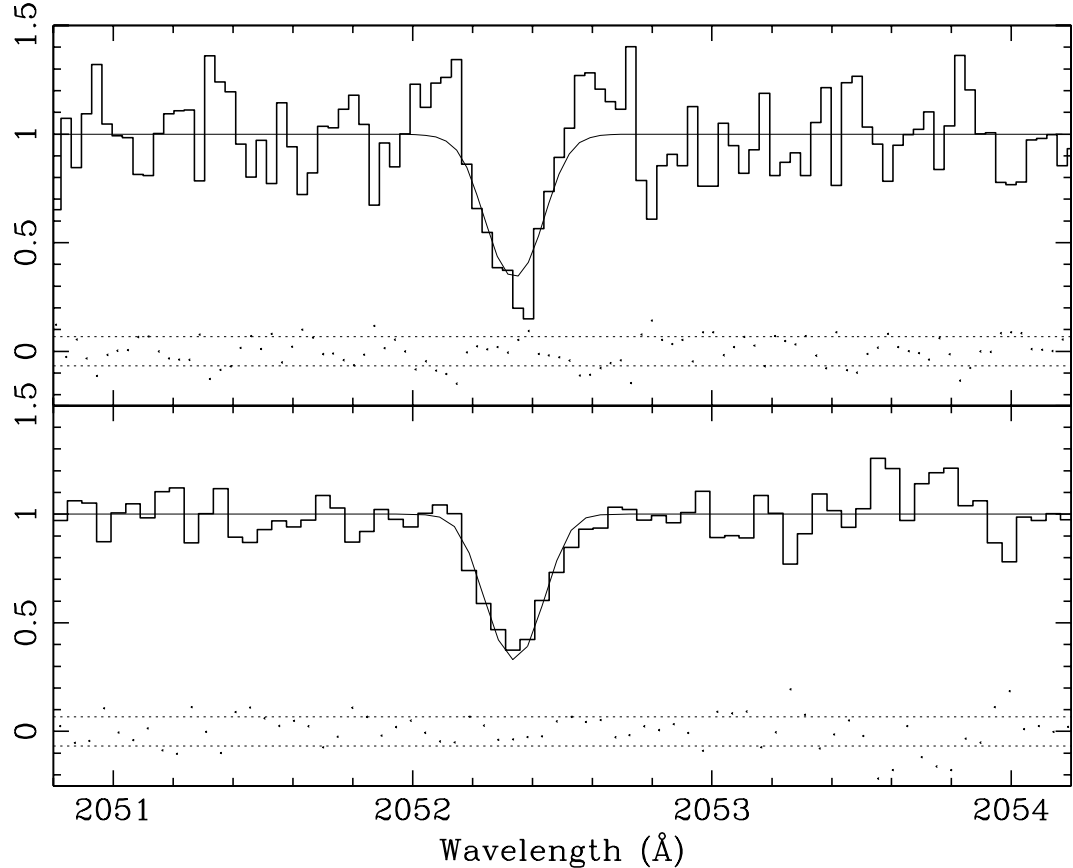


**Figure 3.** The GHRS (above) and STIS (below) spectra covering the  $z = 0.701$  Si III line. The normalised residuals and their  $1\sigma$  error levels are shown centred on  $y = 0$ . The thin curve shows the best fitting solution when both lines are fit simultaneously. This fit provides the parameters in Table 1.

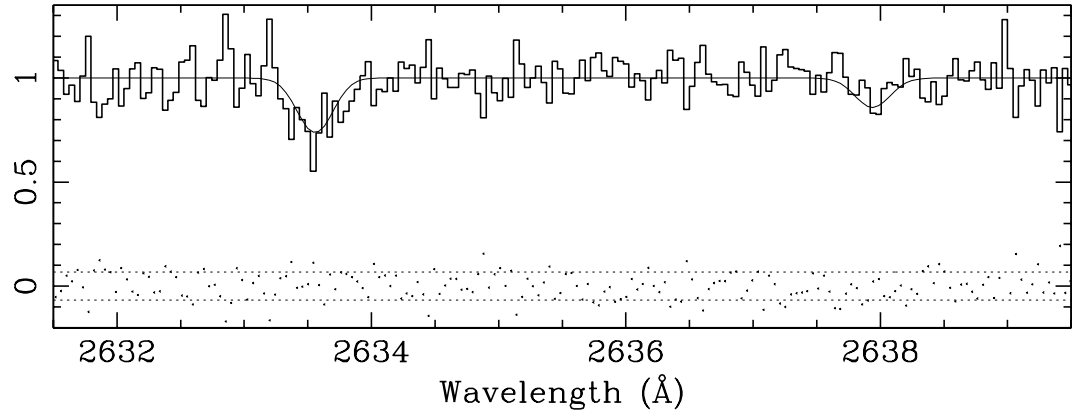


**Figure 4.** A tentative detection of the  $z = 0.701$  4 doublet in the STIS E230M spectrum. The normalised residuals and their  $1\sigma$  error levels are shown centred on  $y = 0$ . The thin curve shows the best fitting solution when both lines of the doublet are fit simultaneously. This fit provides the parameters in Table 1.

redshift of the main H I component is determined by the higher order Lyman series lines in the G140M spectrum. Introducing a shift between the G140M and E230M spectra means that the position of the main H I absorption in the Ly $\alpha$  line changes. To compensate for this change in position, the parameters of the putative D I and the red H I component are also changed. We describe the effect of these shifts on the parameters of the putative D I in section 2.9.

## 2.6 Contamination of the $z = 0.701$ system by systems at other redshifts

We attempt to identify all lines in the E230M spectrum to determine if the  $z = 0.701$  absorption lines are contaminated by H I or metal lines from systems at different redshifts. There are six absorption systems with  $\log[N(\text{H I})] > 14.5$  present in the E230M spectrum. They are at redshifts of 1.0867, 1.0674, 1.0549, 1.0318, 0.7247 and 0.5272. The Ly $\beta$  line at  $z = 0.5272$  falls at  $\sim 1566.5\text{\AA}$ , and may contribute

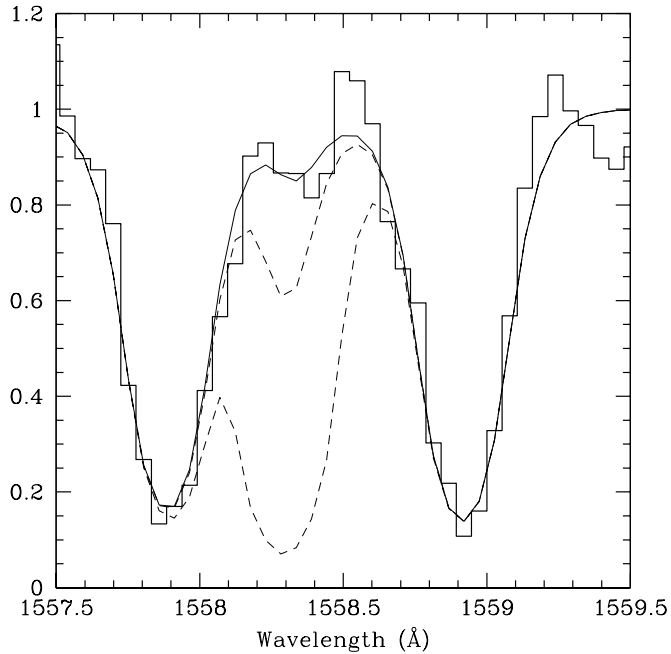


**Figure 5.** A section of the STIS G140M spectrum showing the constraints on the column density of the  $z = 0.602$  absorption system. The thin solid curve is the best fit obtained by including all H<sub>I</sub> components from the  $z = 0.70108$  system and a single component at  $z = 0.6023$ . The middle dashed curve shows the  $z = 0.6023$  column density set at the  $2\sigma$  upper limit. The lower dashed curve shows the column density set to  $\log[N(\text{H I})] = 16.7$ , given in Tytler et al. (1999). The  $b$  parameter for the  $z = 0.6023$  line cannot be well determined by the data and was fixed at  $15 \text{ km s}^{-1}$ . Increasing the  $b$  parameter decreases the upper limit on the  $z = 0.6023$  column density.

to the absorption seen at this wavelength in the G140M spectrum (see Fig. 1). We did not include the region with this absorption when we fitted the G140M spectrum. For each  $\log[N(\text{H I})] > 14.5$  system we searched the wavelength ranges covered by the G140M and E230M spectra for strong associated metal lines that may contaminate the  $z = 0.701$  absorption lines, including Si II, N IV, O I and C II. Only two systems show any strong metal lines: the  $z = 1.0867$  system has associated Si III absorption, and the  $z = 1.0318$  system shows N V absorption. Galactic Fe II and Mn II absorption is also present. We found no other strong metal lines or higher order Lyman H<sub>I</sub> transitions that may be blended with the  $z = 0.701$  lines and affect our analysis.

## 2.7 $z = 0.602$ absorption system

Tytler et al. (1999) suggest that there is evidence in the IUE spectra for another Lyman limit system with  $\log[N(\text{H I})] \simeq 16.7$  at  $z = 0.602$ . It is important to determine whether such a system is present, since if it is, its Ly- $\gamma$  line will fall at  $\sim 1558 \text{ \AA}$  and may blend with the Ly-13 or Ly-14 lines of the  $z = 0.701$  system. Such a Lyman limit system should have a Ly $\alpha$  line at  $\sim 1947 \text{ \AA}$ . The STIS E230M spectra covers this region, although the signal to noise is poor ( $\sim 3$ ). A strong line does appear at  $1948 \text{ \AA}$ , but the low S/N and contamination from a higher redshift H<sub>I</sub> Ly $\beta$  line mean the column density cannot be determined from this line alone.

However, we can put an upper limit on the column density of the suspected  $z = 0.602$  system in the following way. We fitted the  $z = 0.701$  Lyman limit and higher order lines, excluding the lines possibly blended with the  $z = 0.602$  Ly- $\gamma$  line. Then we compared the predicted Ly-13 and Ly-14 lines with the absorption seen, assuming any residual absorption in these two lines is due to the  $z = 0.602$  Ly- $\gamma$  line. Combining the constraints from the low S/N Ly $\alpha$  line and the method above, we find that the contaminating system has a redshift of  $0.6023 \pm 0.00003$ , placing it between the  $z = 0.701$  Ly-13 and Ly-14 lines with  $\log[N(\text{H I})] < 14.54$  (99.7% confidence). The  $z = 0.602$  system does not affect the measured parameters of the  $z = 0.701$  system, as illustrated in Fig. 2.7. No metal lines were detected at  $z = 0.602$ .

## 2.8 Voigt profile fitting

Voigt profiles were fitted to the absorption lines and the best fitting parameters were determined by minimising the  $\chi^2$  statistic. The program VPFIT<sup>4</sup> was used for all line profile fitting. The absorption lines that were detected and fitted in the  $z = 0.701$  system in the STIS spectra are the Ly $\alpha$  line, the Lyman series from Ly- $\epsilon$  to the Lyman limit, Si III (1206.5  $\text{\AA}$ ) and the 4 doublet (1548.2 and 1550.8  $\text{\AA}$ ). The GHRS spectrum covers the Ly $\alpha$  and Si III lines. We fitted all parameters for case (1) described in section 2.5, for no shift between the STIS spectra. The 0.3 pixel error in the uncertainty in the STIS wavelength calibrations is listed after the statistical error in Table 1 for the lines it applies to. We look at the effect of the shifts between the STIS spectra wavelength calibrations on the putative D I's parameters in section 2.9.

The parameters of the main H<sub>I</sub> component are tightly constrained by the unsaturated H<sub>I</sub> higher order lines and the drop in flux at the grey Lyman limit. The main uncertainties in this case are the position of the continuum and the accuracy of the STIS wavelength calibration. Table 1 shows the best fitted parameters to the main H<sub>I</sub> component. The error in redshift due to the error in STIS zero point wavelength calibration is given after the statistical error. The first error for each parameter given in the table is the quadrature addition of the statistical fitting error and the continuum placement error, where applicable.

The Si III line parameters were found by fitting the GHRS and STIS spectra simultaneously. Again we include separately the statistical error in redshift and the error when the wavelength calibration uncertainty of the STIS E230M spectrum is taken into account. The Si III line is offset bluewards from the main H<sub>I</sub> system by  $0.5 \pm 1$  (statistical)  $\text{km s}^{-1}$ .

The 4 line parameters were found by fitting the 4 doublet in the STIS E230M spectra. The statistical error and error due to wavelength calibration are shown separately. The 4 lines are offset bluewards from the main H<sub>I</sub> component by  $4 \pm 3$  (statistical)  $\text{km s}^{-1}$ . The best fitting  $b$  parameter for 4 is large compared to  $b(\text{Mg II})$  and  $b(\text{Si III})$ . This difference is also seen in many damped Ly $\alpha$  absorbers (Wolfe & Prochaska 2000) and is probably due to 4 having a much higher ionization energy than Si III and Mg II, and

<sup>4</sup> Carswell et al., <http://www.ast.cam.ac.uk/~rfc/vpfit.html>

**Table 1.** The absorption line parameters and their errors given by VPFIT. For the two H<sub>I</sub> and putative D<sub>I</sub> lines these are the best fitting parameters when the STIS Lyman limit and the GHRS and STIS Ly $\alpha$  lines are fit simultaneously. For Si III these are the best fitting parameters when the GHRS and STIS Si III lines are fitted simultaneously. The first errors given are the quadrature addition of the statistical and continuum fitting errors. The second errors for the Si III line, 4 doublet and main H<sub>I</sub> component are the errors due to uncertainty in the wavelength calibration of the STIS spectra (0.3 pixels). Note that the errors for the putative D<sub>I</sub> and H<sub>I</sub> red sub-component are not meaningful (see section 2.9). We list the Mg II parameters published by KTOB based on observations taken with Keck/HIRES. The error for  $b(\text{Mg II})$  is our estimate of the error based on our simulated spectra (see section 2.8). The error for  $b(\text{Mg II})$  in KTOB is 1.1  $\text{km s}^{-1}$ .

Ion	$\log(N)$ ( $\text{cm}^{-2}$ )	$z$	$b$ ( $\text{km s}^{-1}$ )
H <sub>I</sub>	$17.213 \pm 0.007$	$0.701074 \pm 0.000003 \pm 0.000015$	$22.1 \pm 0.4$
H <sub>I</sub> <sup>a</sup>	13.5	0.70142	19
Putative D <sub>I</sub> <sup>b</sup>	13.88	0.701108	22
Si III	$12.84 \pm 0.05$	$0.701071 \pm 0.000007 \pm 0.000009$	$14 \pm 2$
4	$13.18 \pm 0.08$	$0.701051 \pm 0.000019 \pm 0.000009$	$20 \pm 5$
Mg II	$11.50 \pm 0.05$	$0.701100 \pm 0.000005$	$12.0 \pm 1.4$

<sup>a</sup> VPFIT does not return sensible errors for this H<sub>I</sub> component. The reasons for this are described in section 2.9.

<sup>b</sup> See section 2.9, Fig. 6, 7 and 8 for the putative D<sub>I</sub> parameter errors.

so being associated with a different velocity space in the absorption cloud.

We use the parameters of the Mg II lines given in KTOB. To verify the errors given by KTOB, we generated a synthetic Mg II spectrum from the fitted  $b$ ,  $N$  and  $z$  values they provided, at the same S/N ( $\sim 70$ ) and resolution (8  $\text{km s}^{-1}$  FWHM) as the Mg II spectrum they published. Our  $\sigma(N)$  and  $\sigma(z)$  were very similar to KTOB's, but our  $\sigma(b)$  was larger, 1.4  $\text{km s}^{-1}$  instead of 1.1  $\text{km s}^{-1}$ . We use our larger  $\sigma(b)$  estimate in our analysis. The Mg II lines are offset redwards from the redshift of the main H<sub>I</sub> system by  $5 \pm 1$  (statistical)  $\text{km s}^{-1}$ . The systematic error for the wavelength calibration for Keck/HIRES spectra is  $< 0.5 \text{ km s}^{-1}$ . This 5  $\text{km s}^{-1}$  shift may be due in part to an error in the STIS wavelength calibration (the 0.3 pixel error in wavelength calibration we consider corresponds to a velocity error of  $\sim 3 \text{ km s}^{-1}$ ). Even though we are not sure of the cause of this shift, it does not affect our analysis, since we use only the Mg II  $b$  parameter (section 2.10).

We attempted to fit the LL and both Ly $\alpha$  lines with a single H<sub>I</sub> component. The minimum reduced  $\chi^2 \equiv \chi^2_{\text{min}}/(\text{no. of degrees of freedom})$  for this fit was 1.7. This fit predicted too much absorption in the higher order lines, and could not account for extra absorption in the red and blue wings of the Ly $\alpha$  line. We needed to add two extra absorption lines, one H<sub>I</sub> sub-component to the red of the main component, and a putative D<sub>I</sub> line to the blue, to find an acceptable reduced  $\chi^2$  (1.04). Table 1 gives the parameters of the red and blue H<sub>I</sub> components.

## 2.9 The errors on the parameters for the putative D<sub>I</sub>

The  $1\sigma$  errors on the parameters in Table 1 are those calculated by VPFIT. These errors are based on the assumptions that (1): the model we have chosen (a single main H<sub>I</sub> component with a red and blue sub-component on either side) is correct and (2): the fitted parameters are independent and

the shape of the  $\chi^2$  parameter space around the minimum  $\chi^2$  is parabolic. However, for the putative D<sub>I</sub> the column density,  $b$  parameter and redshift are correlated. In addition, the  $\chi^2$  parameter space is asymmetric (see Fig. 6, 7 and 8). This is due to the small number of data points that are available to constrain the parameters of the putative D<sub>I</sub>. It may also be due to the difference in 'shape' between the STIS and GHRS Ly $\alpha$  lines (see Figure 2). For these reasons, the  $1\sigma$  estimates given by VPFIT for the putative D<sub>I</sub> parameters may not be accurate. This is also likely to be the case for the red H<sub>I</sub> sub-component. For the other lines (the main H<sub>I</sub> component, Si III, 4, and Mg II), the  $1\sigma$  errors given by VPFIT will be sufficiently accurate.

We find a robust parameter error estimate for the D<sub>I</sub> parameters by using  $\Delta\chi^2$  probability contour maps. These are generated by fixing two parameters (for instance, the  $b$  parameter and redshift of the putative D<sub>I</sub>) and then varying the remaining parameters (the column density of the putative D<sub>I</sub> and all the parameters of the main H<sub>I</sub> component and red H<sub>I</sub> component) to minimise  $\chi^2$ . This creates a grid of  $\chi^2$  values. The distribution of  $\Delta\chi^2 \equiv \chi^2 - \chi^2_{\text{min}}$  is the same as that of a  $\chi^2$  distribution with a number of degrees of freedom equal to the number of fixed parameters (in this case, two). Here  $\chi^2_{\text{min}}$  is the smallest value of  $\chi^2$  for a particular grid. Provided that errors on the data points are normally distributed, the probability contours generated in this way will be correct, irrespective of correlations between the fitted parameters (Cash 1976). We also need to consider the effect the shifts between the STIS E230M spectra have on the D<sub>I</sub> parameters. To do this we again consider the three shifts described in the previous section. Fig. 6, 7 and 8 show the probability contour maps for the three parameters of the putative D<sub>I</sub> for the three different relative shifts between the STIS Lyman limit and Ly $\alpha$  spectra, representing the uncertainty in the wavelength calibration between the two spectra.

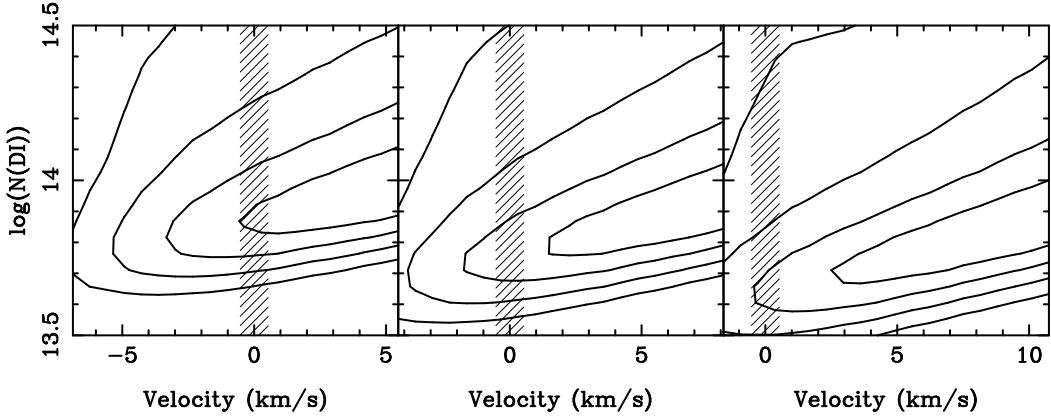


**Figure 6.**  $\log_{10}(N[\text{H}\,\text{I}])$  versus velocity for the putative D1. For the left graph the Lyman limit is shifted 0.3 pixels redwards and the Ly $\alpha$  lines are shifted 0.3 pixels bluewards. For the right graph the Lyman limit is shifted 0.3 pixels bluewards and the Ly $\alpha$  lines are shifted 0.3 pixels redwards. For the centre graph the Lyman limit and Ly $\alpha$  lines are fitted with no shift. The velocity zero point corresponds to  $81.6 \text{ km s}^{-1}$  blueward of the best fitting position of the main H1 component, where we expect D1 to be. The contours represent, from innermost to outermost, the 68.4%, 95.4%, 99.73% and 99.99% confidence levels. The vertical hashed region represents the 68.4% confidence region on the position of the main H1 component.

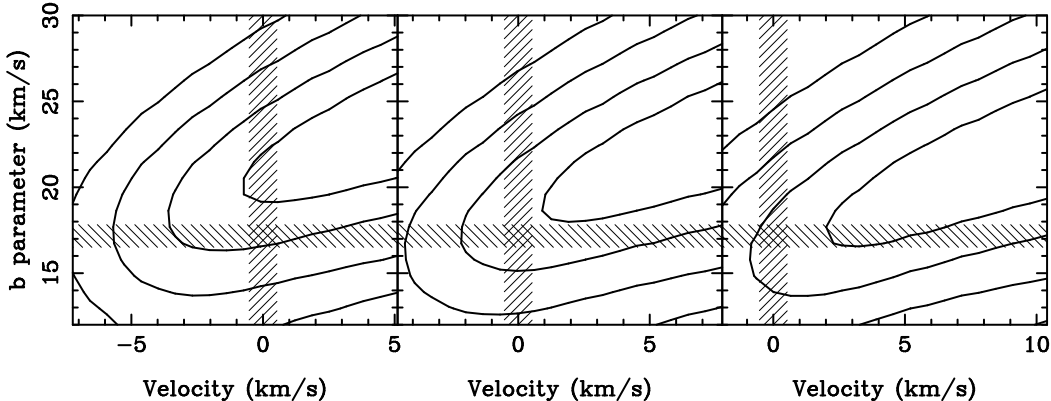


**Figure 7.**  $b$  parameter versus velocity for the putative D1. For the left graph the Lyman limit is shifted 0.1 pixels redwards and the Ly $\alpha$  lines are shifted 0.3 pixels bluewards. For the right graph the Lyman limit is shifted 0.3 pixels bluewards and the Ly $\alpha$  lines are shifted 0.3 pixels redwards. For the centre graph the Lyman limit and Ly $\alpha$  lines are fitted with no shift. The velocity zero point corresponds to  $81.6 \text{ km s}^{-1}$  blueward of the best fitting position of the main H1 component, where we expect D1 to be. The contours represent, from innermost to outermost, the 68.4%, 95.4%, 99.73% and 99.99% confidence levels. The vertical hashed region represents the 68.4% confidence region on the position of the main H1 component. The horizontal hashed region represents the 68.4% confidence region for the D1  $b$  parameter predicted by the H1, Si III and Mg II (see Fig. 9).

## 2.10 The putative D1's $b$ parameter

We can predict what the  $b$  parameter of a D1 line associated with the main H1 absorption from the  $b$  parameters of the Si III, Mg II and main H1 component. This is done by measuring the thermal line broadening,  $b_{\text{therm}}$ , and turbulent broadening,  $b_{\text{turb}}$ , by using the  $b$  parameters from all available ions. If we assume the absorbing cloud has a thermal Maxwell-Boltzmann distribution and any turbulence can be described by a Gaussian velocity distribution, then the  $b$  parameter for a particular ion will be given by

$$b_{\text{ion}}^2 = b_{\text{therm}}^2 + b_{\text{turb}}^2. \quad (1)$$

Here  $b_{\text{therm}}^2 = \frac{2kT}{m}$ , where  $T$  is the temperature of the gas cloud,  $m$  is the mass of the absorbing ion and  $k$  is Boltzmann's constant.  $b_{\text{turb}}^2$  represents the Gaussian broadening

due to small scale turbulence, and is the same for all ionic species.  $b_{\text{therm}}^2$  is proportional to the inverse of the ion mass. We plot  $b^2$  against inverse ion mass in Fig. 9. Subject to the assumptions above, all the ions in the same cloud velocity space should lie on a straight line whose intercept gives  $b_{\text{turb}}$  and slope gives the cloud temperature. Since Mg II and H1 have very similar ionization potentials (IP) (13.6 eV and 15.0 eV respectively), they should trace out the same gas. The IP of Si III is somewhat higher (33.5 eV), but there is evidence that 'intermediate' IP ions, such as Al III, have a similar velocity structure to lower IP ions, such as Mg II (Wolfe & Prochaska 2000). We assume that the Mg II and Si III lines are in the same gas as the H1 and fit least squares line of best fit to these three points. This is shown as the dashed line in Fig. 9. If we use KTOB's estimate for Mg II  $\sigma(b)$ . The D1 point is plotted with its  $1\sigma$  error bars as given

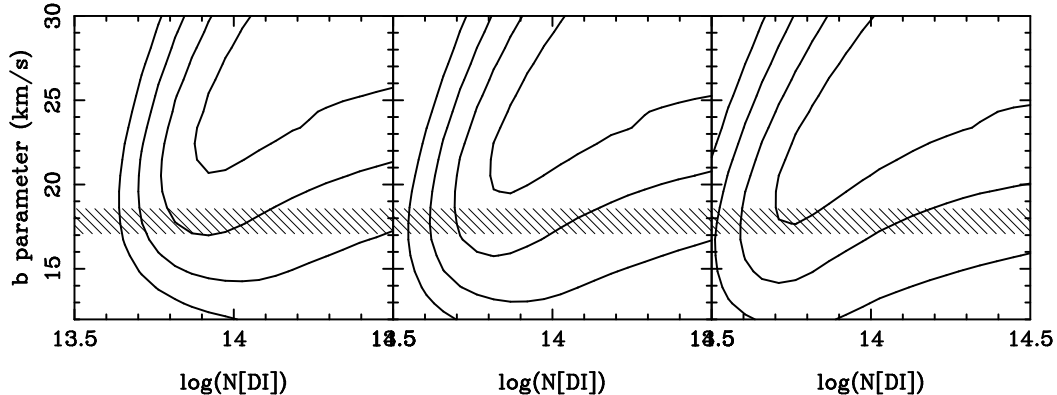


**Figure 8.**  $b$  parameter versus  $\log_{10}(N[\text{H}\text{I}])$  for the putative  $\text{D}\text{I}$ . For the left graph the Lyman limit is shifted 0.3 pixels redwards and the  $\text{Ly}\alpha$  lines are shifted 0.3 pixels bluewards. For the right graph the Lyman limit is shifted 0.3 pixels bluewards and the  $\text{Ly}\alpha$  lines are shifted 0.3 pixels redwards. For the centre graph the Lyman limit and  $\text{Ly}\alpha$  lines are fitted with no shift. The contours represent, from innermost to outermost, the 68.4%, 95.4%, 99.73% and 99.99% confidence levels. The horizontal hashed region represents the 68.4% confidence region for the  $\text{D}\text{I}$   $b$  parameter predicted by the  $b$  parameters of  $\text{H}\text{I}$ ,  $\text{Si}\text{III}$  and  $\text{Mg}\text{II}$  (see Fig 9).

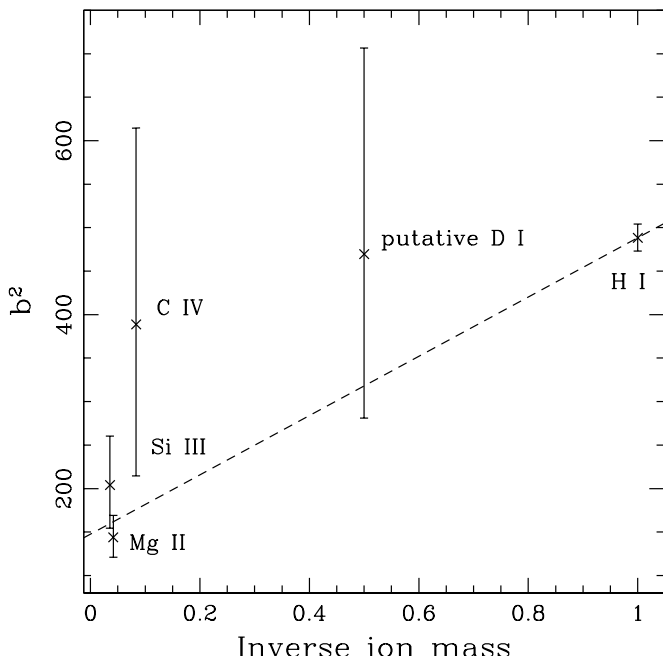


**Figure 9.** The  $b$  parameter squared ( $\text{km}\text{s}^{-1}$ ) $^2$  versus the inverse ion mass ( $\text{amu}^{-1}$ ). The dashed line is the least squares line of best fit to the  $\text{Mg}\text{II}$ ,  $\text{Si}\text{III}$ , and  $\text{H}\text{I}$  points. The putative  $\text{D}\text{I}$  are shown for comparison. The error bars in each case are calculated from the  $1\sigma$  errors given by VPFIT. Note that the  $\text{D}\text{I}$  error bars are not particularly meaningful (see section 2.9). The contour plots shown in Fig 6, 7 and 8 are required to determine whether  $b(\text{D}\text{I})$  is consistent with  $b(\text{H}\text{I})$ ,  $b(\text{Mg}\text{II})$  and  $b(\text{Si}\text{III})$ .

by VPFIT. We find a temperature of  $2.05 \pm 0.12 \times 10^4 \text{ K}$  and a turbulent broadening of  $12.1 \pm 1.3 \text{ km}\text{s}^{-1}$ . Although we use our estimate of  $\text{Mg}\text{II} \sigma(b)$  rather than KTOB's, if we do use KTOB's  $\text{Mg}\text{II} \sigma(b)$ , the derived temperature and turbulent broadening do not change significantly.

## 2.11 Is the blue $\text{H}\text{I}$ component deuterium?

If the blue component is  $\text{D}\text{I}$ , it should fall at a redshift corresponding to a velocity difference of  $81.6 \text{ km}\text{s}^{-1}$  bluewards of the main  $\text{H}\text{I}$  component. In addition, it should have a  $b$  parameter consistent with that predicted in the last section.

We use the contour plots described in section 2.9, combined with the  $b$  parameter test in the last section, to see if the putative  $\text{D}\text{I}$  component's parameters are consistent with those of  $\text{D}\text{I}$ . Fig. 6, 7 and 8 show how  $\Delta\chi^2$  changes for a range of  $b$  parameter, redshift and column density values. Note the degeneracy between the parameters, which has a consequence that the errors obtained using VPFIT are not likely to be accurate for the  $\text{D}\text{I}$ . The hashed bands on each of the plots show the 68% confidence region that the parameters of the blue component are expected to fall in if it is  $\text{D}\text{I}$ . Fig. 7 best illustrates the situation — if the blue component is  $\text{D}\text{I}$ , we would expect its redshift to be the same as that of the main  $\text{H}\text{I}$  component ( $0 \text{ km}\text{s}^{-1}$  velocity difference) and the  $b$  parameter to be consistent with the  $b$  parameters of the  $\text{H}\text{I}$  and metal lines ( $\sim 17 \text{ km}\text{s}^{-1}$ ).

For the left case of Fig. 7, corresponding to a fixed relative shift between the G140M and E230M spectra, we can see that the  $b$  parameter is completely consistent with that of  $\text{D}\text{I}$ , but the redshift is inconsistent. For the right case, the redshift is consistent, but the  $b$  parameter is not. Where there is no relative wavelength shift between the spectra, the parameters of the blue component are inconsistent at a  $\sim 80\%$  confidence level. While these results do not suggest that the blue component is  $\text{D}\text{I}$ , they do not conclusively show that is not  $\text{D}\text{I}$ .

If we take the case of no shift between the G140M and E230M spectra and *assume* the blue absorption is entirely due to  $\text{D}\text{I}$ , fixing the  $b$  parameter and redshift at those we expect for  $\text{D}\text{I}$ , we find the ratio  $\text{D}/\text{H} = (3.0 - 4.6) \times 10^{-4}$  ( $1\sigma$  limit).

## 2.12 Comparison with previous analyses of this system

We have analysed this absorption system using the same spectra presented in Webb et al. (1997), Tytler et al. (1999) and KTOB, considering important systematic effects not addressed in these previous analyses.

There are several small differences in our fitted parameters for the main H I component, putative D I component and Si III line compared to KTOB's fitted parameters. Our line spread function is slightly different from KTOB's and we use a larger error for  $b(\text{Mg II})$  (see section 2.8). We have explored the effect that relative shifts between the wavelength scales of the G140M and E230M STIS spectra have on the parameters of the putative D I line. However, none of these effects substantially change the conclusions of KTOB. As can be seen from Fig. 7, if a large relative shift between the G140M and E230M wavelength scales is present, the probability that the putative D I really is D I is decreased.

The most important reason for our different result from KTOB is a difference in generating our probability contours in Fig. 6, 7 and 8. When generating our  $\chi^2$  contours, we varied all the parameters of all the components in the  $z = 0.7$  complex. To generate the plot in KTOB's Fig. 7, when calculating the minimum  $\chi^2$  only the column density of the putative D I component was varied. The remaining putative D I parameters and all the parameters of the main H I component and the red H I sub-component were fixed by KTOB. This means their contours do not accurately represent the actual range of probabilities for the putative D I  $b$  parameter and redshift. The true confidence ranges are somewhat larger. This is the main reason we find that the putative D I parameters are inconsistent with those expected for D I at the  $\sim 80\%$  rather than  $> 98\%$  level.

Our D/H upper limit calculated assuming the blue absorption is entirely due to D I is, not surprisingly, consistent with the Tytler et al. (1999) upper limit of  $5.7 \times 10^{-4}$ .

## 3 DISCUSSION

We have analysed the  $z = 0.701$  absorption complex towards PG 1718+4801 using HST STIS and GHRS spectra, considering systematic errors that were neglected in previous analyses. The most important of these systematic errors is the absolute wavelength calibration of the STIS G140M and E230M spectra. Introducing a relative shift, comparable to the wavelength error, between these two sets of spectra significantly alters the parameters of the putative D I.

We find that the parameters of the absorption line previously identified as D I are marginally inconsistent with those expected. In particular, the  $b$ -parameter and line position of this feature are at best consistent with the expected values at the 20% level.

We have shown that the absorption system at  $z = 0.602$ , previously claimed as having  $\log[N(\text{H I})] \simeq 16.7$  in fact has  $\log[N(\text{H I})] < 14.5$ .

If we assume that the blue component is D I, we find D/H =  $(3.0 - 4.2) \times 10^{-4}$ . If significant contamination is present, then of course D/H may be significantly lower than  $3.0 \times 10^{-4}$ .

The D/H range given here corresponds to a  $1\sigma$  range

for  $\Omega_b h^2$  of  $0.003 - 0.006$ . We can compare this range with  $\Omega_b h^2$  estimates from other sources. Two recent estimates of the primordial Li<sup>7</sup>/H abundance are  $(0.91 - 1.91) \times 10^{-10}$  (Ryan, Beers, Olive, Fields & Norris 2000) and  $(1.92 - 2.49) \times 10^{-10}$  (Bonifacio 2002). Combining these two ranges, we find  $\text{Li}^7(\Omega_b h^2) = 0.0044 - 0.020$ . Two samples recently used to measure the He<sup>4</sup> abundance,  $Y_P$ , give  $0.238 \pm 0.003$  (The sample in Izotov & Thuan 1998, using the ionization correction factor in Gruenwald, Steigman & Viegas 2002) and  $0.2405 \pm 0.0017$  (Peimbert, Peimbert & Ruiz 2000). Taking the highest and lowest limits of these two ranges gives  $\text{He}^4(\Omega_b h^2) = 0.0065 - 0.0145$ . Sievers et al. (2002) give CMB( $\Omega_b h^2$ ) =  $0.023 \pm 0.003$  based on all currently available CMB data. Taking an average of the five D/H measurements made in other QSO absorption clouds, weighted by their inverse variances, gives D( $\Omega_b h^2$ ) =  $0.021 \pm 0.001$ .

The  $\Omega_b h^2$  range for the  $z = 0.701$  QSO absorber is consistent with the Li<sup>7</sup> range and only marginally inconsistent with the He<sup>4</sup> range. It is significantly inconsistent with both the CMB and low QSO D/H  $\Omega_b h^2$  ranges, however. The metallicity of this absorber is low,  $[\text{Si}/\text{H}] = -2.4$  (Tytler et al. 1999), and the QSO absorption systems used to measure D/H have similarly low metallicities. At these metallicities no significant astration is thought to have occurred and the measured D/H values should be primordial. For a standard homogenous BBN, we expect the primordial D/H to be independent of direction and redshift. Thus the inconsistency of the  $z = 0.701$  D/H value with lower D/H values in other QSOs and the CMB  $\Omega_b h^2$  value supports the argument that the putative D I in this system is contaminated with H I.

However there are several caveats. Only five D/H measurements in QSO absorbers have been made. Even among these 'low' D/H values there is considerable scatter, which is not expected based on the standard BBN, no astration picture. This is may be due to unaccounted for systematic errors, but other explanations have been suggested. Fields, Olive, Silk, Cassé & Vangioni-Flam (2001) suggest the scatter may be evidence for an early population of stars that have caused astration even in these low metallicity absorbers. Jedamzik (2002) suggest it is possible that there may be rare astrophysical sites where D/H has been enhanced above the primordial value. It would be imprudent to reject entirely the possibility that this system shows a high D/H until further D/H measurements in QSO absorbers are available, particularly if there is a trend of D/H with metallicity.

We acknowledge helpful comments from Michael Murphy and Mike Irwin, and correspondence regarding STIS wavelength calibration with Claus Leitherer at the STScI. We also thank Gary Steigman for his helpful correspondence, and the referee for his suggestions on how to improve the paper.

## REFERENCES

- Adams T. F., 1976, A&A, 50, 461
- Bonifacio P., 2002, A&A, 395, 515
- Cash W., 1976, A&A, 52, 307
- Epstein R. I., Lattimer J. M., Schramm D. N., 1974, Nat, 263, 198

Fields B. D., Olive K. A., Silk J., Cassé M., Vangioni-Flam E., 2001, ApJ, 563, 653

Gruenwald R., Steigman G., Viegas S. M., 2002, ApJ, 567, 931

Izotov Y. I., Thuan T. X., 1998, ApJ, 500, 188

Jedamzik K., 2002, Planetary and Space Science, 50, 1239

Kirkman D., Tytler D., O'Meara J. M., Burles S., Lubin D., Suzuki N., Carswell R. F., Turner M. S., Wampler E. J., 2001, ApJ, 559, 23

Kirkman D., Tytler D., Suzuki N., O'Meara J., Lubin D., 2003, astro-ph/0302006

Lanzetta K. M., Turnshek D. A., Sandoval J., 1993, ApJS, 84, 109

Levshakov S. A., Dessauges-Zavadsky M., D'Odorico S., Molaro P., 2002, ApJ, 565, 696

O'Meara J. M., Tytler D., Kirkman D., Suzuki N., Prochaska J. X., Lubin D., Wolfe A. M., 2001, ApJ, 552, 718

Peimbert M., Peimbert A., Ruiz M. T., 2000, ApJ, 541, 688

Pettini M., Bowen D. V., 2001, ApJ, 560, 41

Proffitt C., 2002, STIS Instrument Handbook, Version 6.0. STScI, Baltimore STScI

Ryan S. G., Beers T. C., Olive K. A., Fields B. D., Norris J. E., 2000, ApJ, 530, L57

Tytler D., Burles S., Lu L., Fan X., Wolfe A., Savage B. D., 1999, AJ, 117, 63

Webb J. K., Carswell R. F., Irwin M. J., Penston M. V., 1991, MNRAS, 250, 657

Webb J. K., Carswell R. F., Lanzetta K. M., Ferlet R., Lemoine M., Vidal-Madjar A., 1998, in Structure et Evolution du Milieu Inter-Galactique Revele par Raies D'Absorption dans le Spectre des Quasars, 13th Colloque d'Astrophysique de l'Institut d'Astrophysique de Paris A High Deuterium Abundance at  $z=0.7$ ; Evidence for Cosmic Inhomogeneity?. pp 345–+

Webb J. K., Carswell R. F., Lanzetta K. M., Ferlet R., Lemoine M., Vidal-Madjar A., Bowen D. V., 1997, Nat, 388, 250

Wolfe A. M., Prochaska J. X., 2000, ApJ, 545, 603